**TOPICAL REVIEW • OPEN ACCESS**

# Modulating short-term and long-term plasticity of polymer-based artificial synapses for neuromorphic computing and beyond

To cite this article: Ui-Chan Jeong *et al* 2024 *Neuromorph. Comput. Eng.* **4** 032001

View the article online for updates and enhancements.

# NEUROMORPHIC
## Computing and Engineering

**TOPICAL REVIEW**

# Modulating short-term and long-term plasticity of polymer-based artificial synapses for neuromorphic computing and beyond

Ui-Chan Jeong[1,4], Jun-Seok Ro[1,4], Hea-Lim Park[1,*] and Tae-Woo Lee[2,3,*]

1 Department of Materials Science and Engineering, Seoul National University of Science and Technology, Seoul 01811, Republic of Korea
2 Department of Materials Science and Engineering, Seoul National University, Seoul 08826, Republic of Korea
3 School of Chemical and Biological Engineering, Institute of Engineering Research, Research Institute of Advanced Materials, Soft Foundry, Seoul National University, 1 Gwanak-ro, Gwanak-gu, Seoul 08826, Republic of Korea
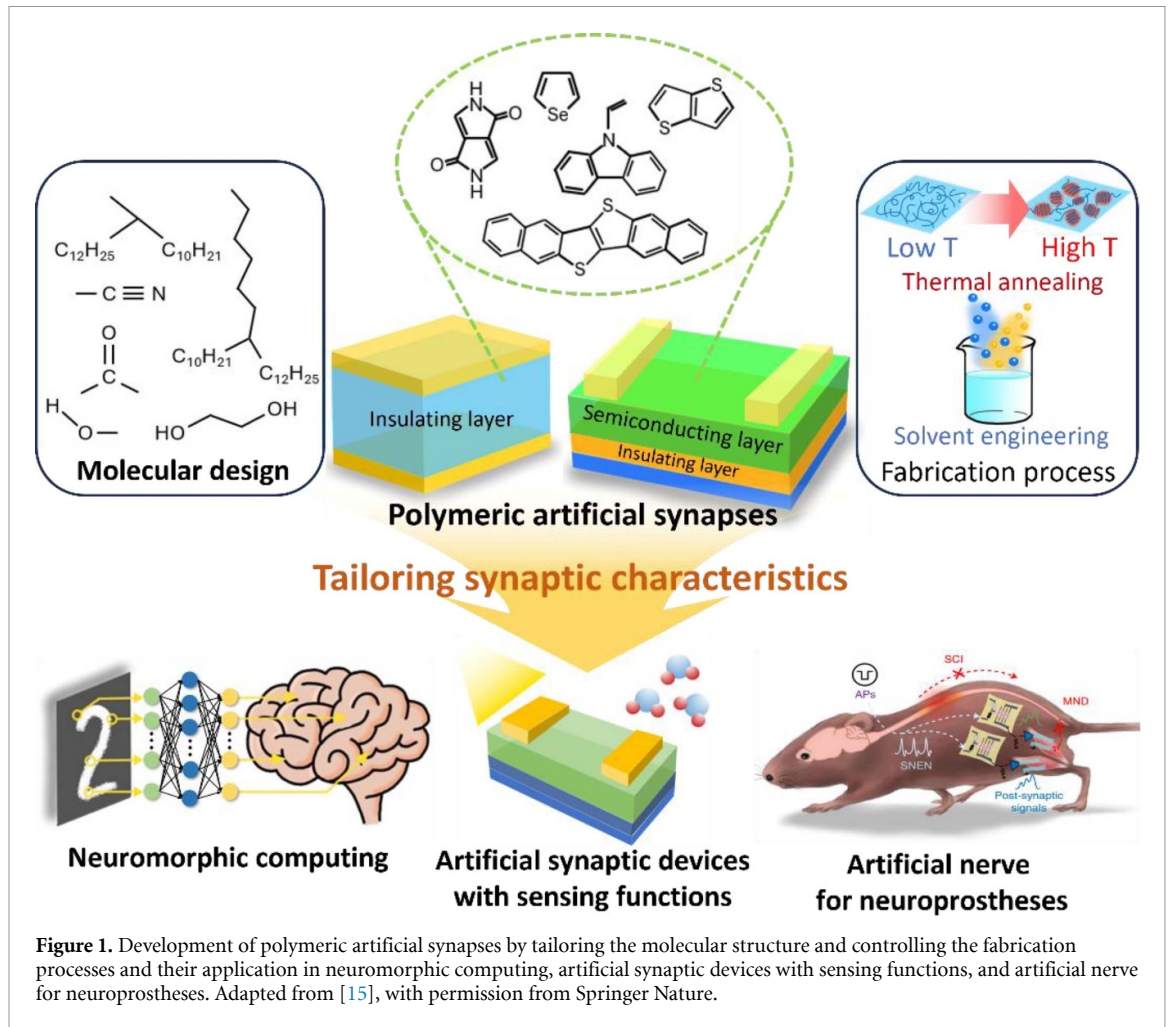* Authors to whom any correspondence should be addressed.
4 These authors contributed equally to this work

E-mail: parkhl21@seoultech.ac.kr and twlees@snu.ac.kr

## Abstract

Neuromorphic devices that emulate biological neural systems have been actively studied to overcome the limitations of conventional von Neumann computing structure. Implementing various synaptic characteristics and decay time in the devices is important for various wearable neuromorphic applications. Polymer-based artificial synapses have been proposed as a solution to satisfy these requirements. Owing to the characteristics of polymer conjugated materials, such as easily tunable optical/electrical properties, mechanical flexibility, and biocompatibility, polymer-based synaptic devices are investigated to demonstrate their ultimate applications replicating biological nervous systems. In this review, we discuss various synaptic properties of artificial synaptic devices, including the operating mechanisms of synaptic devices. Furthermore, we review recent studies on polymer-based synaptic devices, focusing on strategies that modulate synaptic plasticity and synaptic decay time by changing the polymer structure and fabrication process. Finally, we show how the modulation of the synaptic properties can be applied to three major categories of these devices, including neuromorphic computing, artificial synaptic devices with sensing functions, and artificial nerves for neuroprostheses.

## 1. Introduction

Recently, as the amount of information has increased with the growing demand for artificial intelligence (AI) and internet of things (IoT), neuromorphic devices have been developed to mimic biological nervous systems, enabling parallel data processing with significantly lower power consumption [1–3]. Among the various materials that compose neuromorphic devices, polymer conjugated materials are attracting attention due to their advantages such as easily tunable optical/electrical properties, flexibility, and biocompatibility. Due to these advantages, polymers are essential material for applications such as wearable electronics, smart sensors for IoT, and neuroprosthetic devices, which can detect physiological signals and/or process large amounts of analog signals received from the external environment. To perform these functions, neuromorphic devices should be seamlessly integrated with biological systems, whether attached to the curved surfaces of the body or implanted internally. Therefore, polymer-based neuromorphic devices using polymer conjugated materials are being actively studied for state-of-the-art neuromorphic applications.

Among neuromorphic devices, artificial synapses that mimic biological synapses are crucial for replicating brain learning and memory behaviors [4–9]. Biological synapses manage learning and memory by controlling synaptic strength, known as synaptic plasticity, which is the strength of the connection between synapses. Typically, various synaptic plasticity of artificial synapses can be adjusted by the retention or decay time of the synaptic current [10]. To enable artificial synapses to perform functions ranging from

**Figure 1.** Development of polymeric artificial synapses by tailoring the molecular structure and controlling the fabrication processes and their application in neuromorphic computing, artificial synaptic devices with sensing functions, and artificial nerve for neuroprostheses. Adapted from [15], with permission from Springer Nature.

simple calculations to complex learning and memory, a wide range of decay time is required [11, 12]. Consequently, controlling the decay time of polymer-based artificial synapses is of great importance, prompting numerous related studies. Because polymers allow for molecular design modulation and device performance control through various fabrication processes parameters (i.e. annealing temperature, crosslinking processes, and solvent combination), many studies have explored expressing a wide range of decay times through these methods (figure 1) [13, 14].

Herein, we first introduce the various biological synaptic properties, which are demonstrated by artificial synapses, including the operating mechanism of the devices. Next, various strategies for controlling synaptic plasticity in polymer-based artificial synapses are reviewed in terms of changing the molecular structure and fabrication processes. Finally, we introduce various applications of polymer-based synaptic devices. These applications are largely categorized into neuromorphic computing, artificial synaptic devices with sensing functions, and artificial nerves for neuroprostheses. The polymer-based neuromorphic devices we introduced are able to implement the desired synaptic characteristics through various strategies, and they would be the basis for the development of state-of-the-art neuromorphic applications.

## 2. Synaptic properties of biological and artificial synaptic devices

Neurons and synapses are the basic elements that make up the nervous system. Neurons consist of cell body (soma), axon, and dendrite. Synapses connect two neurons and function as signal transmitters and processors. Synapses can be classified into two types: electrical synapse and chemical synapse. In electrical synapses, gap junctions between neurons mediate neural signal transmission in the order of 2–4 nm and directly connect the presynaptic and the postsynaptic cells [16]. In chemical synapses, signal transmission between neurons occurs at synaptic clefts in the order of 20–40 nm via the release of a neurotransmitter [17, 18]. For this reason, the structure and operation of the chemical synapse can be explained as follows. When vesicles in presynaptic membranes release a neurotransmitter into the synaptic cleft, they diffuse across the synaptic cleft and bind to receptors of the postsynaptic membrane. Consequently, ion channels are opened,

and ions can spread through the postsynaptic membrane, causing a change in the membrane potential. This membrane potential can then be increased or decreased according to the type of neurotransmitter [16–19]. The increased potential and the decreased membrane potential are referred to as excitatory postsynaptic potential and inhibitory postsynaptic potential, respectively [20]. Synaptic plasticity is defined as the change in synaptic strength between presynaptic and postsynaptic neurons. Moreover, depending on the decay time of synaptic weight, synaptic plasticity is widely categorized into short-term plasticity (STP) and long-term plasticity (LTP), i.e. STP exhibits relatively rapid decay time of synaptic weight and LTP exhibits slow decay time of synaptic weight, which is related to the formation of long-term memory [21–24].

Many synaptic properties have been emulated in artificial synapses to emulate biological synapse in neuromorphic devices. For example, paired-pulse facilitation is a form of STP. When one presynaptic voltage spike is applied, the postsynaptic current increases to a certain level ($A_1$). When two consecutive presynaptic voltage spikes are applied, the current increased by the second spike ($A_2$) is higher than the current increased by the first spike ($A_1$). This is a phenomenon and can be expressed as $100 \times A_2/A_1$ [25, 26]. As the number, amplitude, and frequency of presynaptic voltage spikes increase, the synaptic behavior changes from STP to LTP. Moreover, spike-time-dependent plasticity (STDP) can also modulate synaptic weight [27]. In STDP, because synaptic weight is not only related to the time interval between spikes but also to the order of spike, the synaptic weight can be then modulated by adjusting the time interval and order between spikes. In addition, a phenomenon in which the synaptic weight is modulated by the spiking rate is called spike-rate-dependent plasticity (SRDP). In SRDP, the synaptic weight is strengthened or weakened according to the frequency of the spikes. This behavior is an important rule for updating synaptic weights in learning models. Spike-duration-dependent plasticity can modulate the synaptic weight by changing the duration of spikes [26, 28]. These synaptic characteristics are essential to simulate synaptic behavior of biological neural system. When input signals are applied to a biological synapse, the synaptic weight changes and is multiplied to perform learning, memory, and cognition, and solve an unstructured problem. These are demonstrated through synaptic weight update using learning rules such as STDP and SRDP. Therefore, it is important to implement synaptic plasticity in artificial synapse to process input data and perform various functions. In artificial synapse, these functions can occur simultaneously and allow tasks to be performed with parallel information processing. This method is called neuromorphic computing, which goes beyond the limits of conventional computing in terms of speed and energy consumption while complementing the superior performance and stability of conventional computing.

These synaptic characteristics have been implemented through various mechanisms in artificial synaptic devices. According to device structures, artificial synaptic devices can be divided into two categories, i.e. two-terminal and three-terminal devices. In the two-terminal device, which is referred to as a memristor, the synaptic weight is controlled by the conductivity of the active layer between the top electrode (TE) and the bottom electrode (BE). The TE and BEs are referred to as presynaptic and postsynaptic neurons, respectively, and the active layer is referred to as synapse [29, 30]. A metallic filament (MF) is one of the representative mechanisms among two-terminal devices. When a presynaptic spike is applied at the TE, the active metal is oxidized into metal cations. These metal cations are then transported to the BE through the active layer by an electric field, and are reduced by electrons to form an MF. In this process, the formation of an MF changes conductance; therefore, controlling the formation of an MF can affect synaptic plasticity [31–34]. However, controlling synaptic plasticity in conventional memristors has proven challenging due to the random and stochastic formation of MFs. To address this, studies have focused on suppressing random MF formation and promoting localized MF formation through structural engineering of memristors, thereby enabling control over synaptic plasticity. For instance, inserting a graphene layer as an ion barrier between two electrodes inhibits the formation of random MFs, and the nanoholes generated in the graphene layer facilitate localized MF formation [35]. Additionally, introducing interfacial triggering sites can achieve localized MF formation. When an active metal (e.g. Ag) that is used in the TE is locally deposited on the BE to form a nanocluster structure, MFs preferentially form in this nanostructure, increasing the retention time [36]. Furthermore, ion injection from the TE can be regulated by adjusting its thickness: insufficient ion injection leads to STP due to unstable MF formation, while sufficient ion injection results in long-term potentiation (LTP) due to stable MF formation. This control over ion injection allows for the regulation of synaptic plasticity [33].

Next, three-terminal synaptic devices are referred to as transistors and consist of three terminals (gate, source, and drain electrodes). In an artificial synaptic transistor, channel conductance between source and drain electrodes changes when a presynaptic spike is applied at the gate electrode. Therefore, the synaptic weight can be modulated in transistor by changing the channel conductance. Artificial synaptic transistors are divided into mainly three types based on their operating mechanisms, i.e. ferroelectricity, charge trapping, and ionic doping/dedoping. In ferroelectricity, a ferroelectric gate insulator can be used to emulate the synaptic properties. When a presynaptic spike is applied, the polarization domains of the ferroelectric gate insulators are aligned along the direction of the external electric field. When the electric field is removed,

the change of polarization domain does not disappear instantly and is maintained for a relatively long time [37, 38]. LTP is obtained in ferroelectric-based devices. Moreover, the ferroelectric-based transistor can enhance and diversify the performance of artificial synapses through a dual-gate structure [39, 40]. This design increases the versatility of artificial synapses by mimicking the biological nervous system's ability to simultaneously receives and processes multiple signals. Additionally, this dual-gate structure exhibits superior sensitivity to stimuli compared to the typical single-gate structure and increases synaptic weight change for the same stimuli, thereby enhancing retention time [41–43].

The charge trapping at organic semiconductor (OSC)/insulator interfaces can modulate the synaptic weight [44, 45]. For example, when light stimulation is applied in a photonic synapse, electron–hole pairs are generated, and the characteristics of the insulating layer, such as hydroxyl groups in poly(4-vinylphenol), can lead to the trapping of photogenerated electrons at the OSC/insulator interfaces [46, 47]. Even after the light spike is removed, trapped charges recombined and disappear, exhibiting STP and characteristics. However, it is challenging for the dielectric material to store charges for extended period. To address this, long-term synaptic plasticity can be enhanced by introducing a floating-gate structure. The floating-gate transistor features a floating gate positioned between a blocking dielectric and a tunneling dielectric layer [48]. In the floating-gate transistors, charges are readily trapped in the floating gate when the gate voltage fluctuates due to quantum tunneling effects. The trapped charges in the floating gate, facilitated by the charge-blocking and charge-tunneling layers, are non-volatile. Consequently, channel conductance can be modulated over extended periods through these captured charges, resulting in a delayed decay time [49–51].

Next, the ionic doping/dedoping process can also affect the synaptic weight. For example, an ion-gel-gated polymeric synaptic transistor (IGPST) can modulate the synaptic weight via doping/dedoping. In IGPST, when a presynaptic voltage spike is applied at the gate electrode, the ions of the ion gel move toward an ion-gel/semiconductor interface. The ions are then doped into the semiconducting channel, and the carriers induced by ions accumulate in the semiconducting channel, increasing the postsynaptic current. Removing the voltage spike induces the dedoping of ions from the semiconducting channel to their original positions and leads to decaying of the postsynaptic current. The device shows an LTP when it faces difficulty in diffusing out the doped ions in the channel, whereas it achieves an STP when it rapidly diffuses the doped ions from the channel layer [52–54]. In this regard, the dedoping process of ions can be modulated according to the interaction of ions with semiconducting layers.

# 3. Strategies for various synaptic characteristics

Polymeric synaptic devices that emulate biological synapses have the potential to be applied in neuromorphic applications, such as neuromorphic computing and artificial nerves for neuroprostheses. Because biological synapses indicate different decay time according to their location and function, it is important to implement STP and LTP [55–57]. To express both STP and LTP characteristics in artificial synapses, strategies that modulate the molecular structures, such as polymer backbone and side chain, and fabrication processes, including thermal annealing and solvent engineering, have been reported. Therefore, in this section, we reviewed previous studies on how the molecular structure and fabrication process affect synaptic plasticity.

## 3.1. Molecular structure
Studies have been conducted to modulate the molecular structures of polymers used in semiconducting and insulating layers [13, 58–60]. The change in the side chain or backbone of polymers leads to the modulation of the intermolecular interaction, which can affect the synaptic plasticity of the devices. Therefore, we introduce studies that modulate the synaptic properties by changing the molecular structure of polymers used as semiconductors and insulators.

### 3.1.1. Semiconducting layer
In semiconducting layers, side chain engineering has been adopted to control the synaptic properties. First, a diketopyrrolopyrrole (DPP)/selenophene–vinylene–selenophene (SVS) copolymer was used as the semiconducting layer in IGPST to investigate how the length of the side chain affect synaptic plasticity [54]. Two types of DPP–SVS copolymers, which have different lengths of the alkyl spacers of the side chains, were fabricated. One has a relatively short alkyl spacer group, with 24 carbons in the alkyl side chain (DPP–24SVS), while the other has a long alky spacer group, with 29 carbons in the alkyl side chain (DPP–29SVS). In DPP–29SVS, a relatively long alkyl spacer in the side chain decreases the steric hindrance between bulky branched side chains (figure 2(a)). Therefore, DPP–29SVS exhibited a $\pi$-conjugated close-packed planar structure (high crystallinity). On the contrary, in DPP–24SVS, closely attached alkyl spaces in the side chain interfere the formation of a planar $\pi$-conjugated structure (low crystallinity). Compared with the amorphous region, the $\pi$-conjugated backbone of the crystalline region, which has a
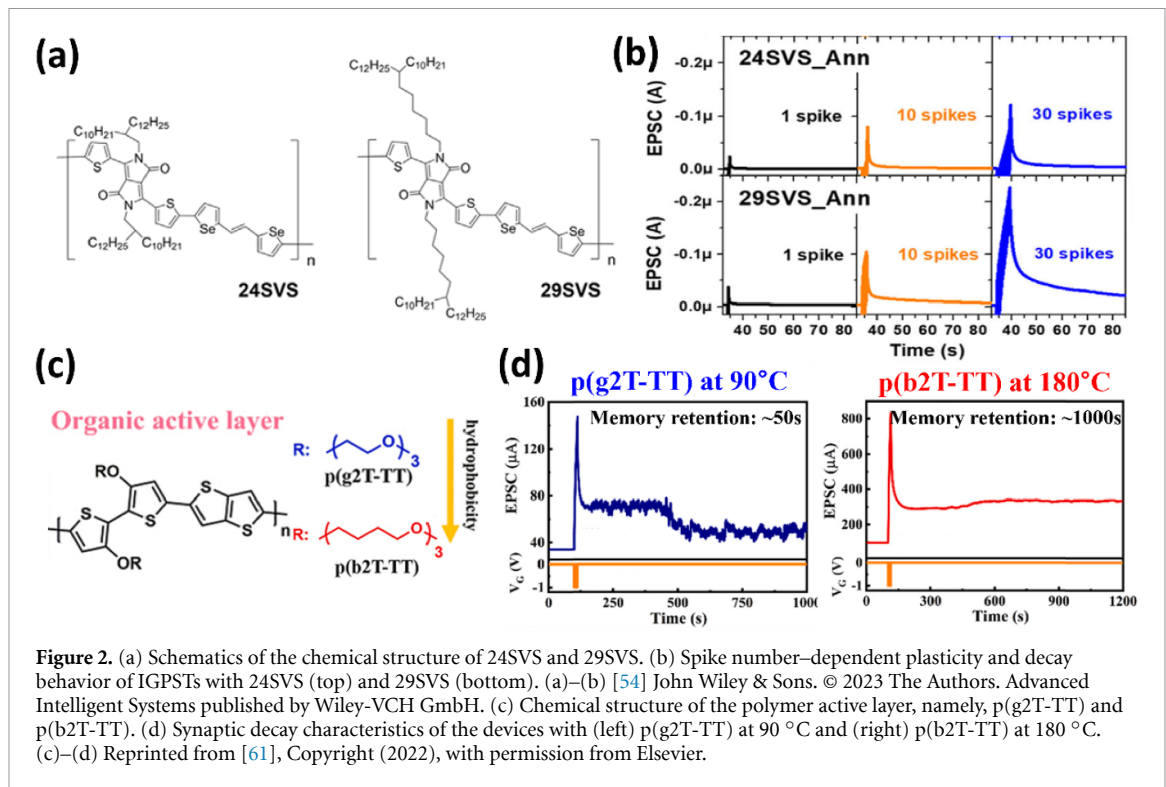
**Figure 2.** (a) Schematics of the chemical structure of 24SVS and 29SVS. (b) Spike number–dependent plasticity and decay behavior of IGPSTs with 24SVS (top) and 29SVS (bottom). (a)–(b) [54] John Wiley & Sons. © 2023 The Authors. Advanced Intelligent Systems published by Wiley-VCH GmbH. (c) Chemical structure of the polymer active layer, namely, p(g2T-TT) and p(b2T-TT). (d) Synaptic decay characteristics of the devices with (left) p(g2T-TT) at 90 °C and (right) p(b2T-TT) at 180 °C. (c)–(d) Reprinted from [61], Copyright (2022), with permission from Elsevier.

strong intermolecular π–π interaction, exhibits higher resistance against ion transport. Therefore, ions doped in the crystalline region are trapped for a long time than those in the amorphous region. Thus, higher crystalline DPP–29SVS exhibited longer decay time of postsynaptic current than DPP–24SVS, corresponding to LTP characteristics (figure 2(b)).

The polymer film is susceptible to external environmental conditions, such as moisture and temperature, which can induce the deformation of the crystal structure; therefore, stable polymer semiconducting materials must be developed to achieve a long retention time of the postsynaptic current [62–64]. Therefore, ethylene glycol (EG) side chain–based p(g2T-TT) and butylene glycol (BG) side chain–based p(b2T-TT) semiconducting layers were investigated with the same bithiophene–thienothiophene backbone (figure 2(c)) [61]. The hydrophobic BG side chain prevents chemical reaction with oxygen and water, minimizing the degradation of electrical properties. Moreover, using BG side chains increases the rigidity of the backbone by providing strong interchain interaction. In this regard, p(b2T-TT) has higher temperature resilience compared to p(g2T-TT). As temperature increases, p(g2T-TT) indicates a relatively large change in a film morphology that degrades the crystalline structure, causing a decrease in the electrical performance of the device. On the contrary, due to the strong interchain interaction of the p(b2T-TT) backbone, p(b2T-TT) exhibited an almost unchanged microstructure at high temperature, resulting in a stable memory retention characteristic (figure 2(d)). Consequently, due to the hydrophobic BG side chain and rigid backbone induced by the BG side chain, p(b2T-TT)-based PST indicated a stable and long retention time and operated well even in harsh environments.

*3.1.2. Insulator layer*

The insulating layers in organic synaptic transistors are important because charges pass through few monolayers above the OSC/insulating interface [65–68]. For example, functional groups of polymeric insulating layers can act as electron trapping sites at OSC/insulator interfaces. Poly(methyl methacrylate) (PMMA), polystyrene (PS), and organosilicon (DC 1-2577) were used as insulating polymers to investigate how functional groups of insulating polymers affect synaptic plasticity [69]. Unlike PS and PMMA, only DC 1-2577 has a hydroxyl group known as the polar group. In DC 1-2577-based synaptic transistors, the dipoles of hydroxyl groups are randomly positioned before a gate voltage is applied. The dipoles are then aligned along the direction of the gate field after gate voltage is applied. The alignment of the dipoles acts as an additional gate bias, inducing more charge carriers at the OSC/dielectric interface and an increase in resultant current. These aligned dipoles do not return to their original state even after disappearance of the gate voltage. Consequently, increased current levels were maintained for a long time, and only DC 1-2577-based synaptic transistors exhibited prolonged decay time of the postsynaptic current. To investigate
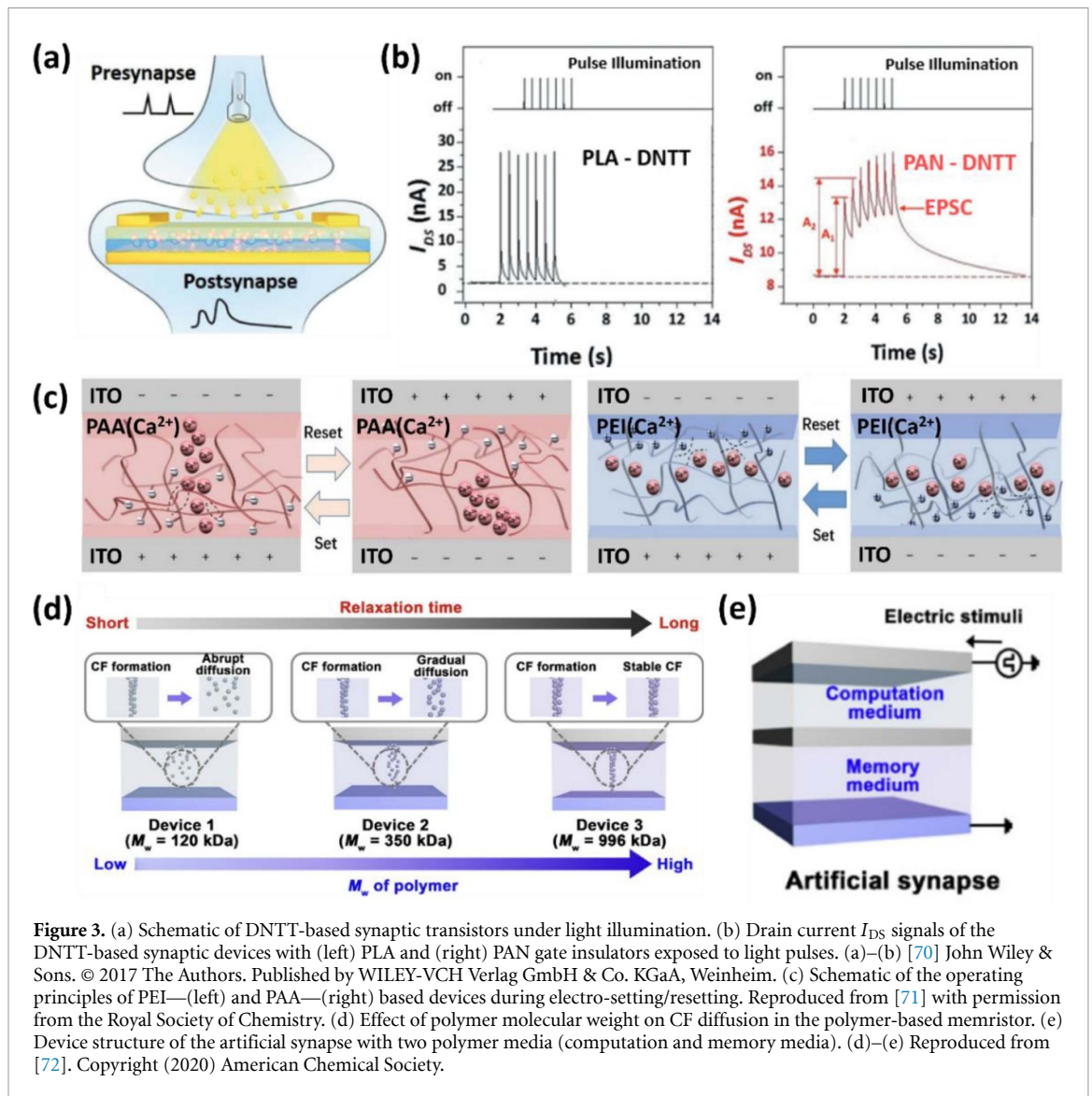
**Figure 3.** (a) Schematic of DNTT-based synaptic transistors under light illumination. (b) Drain current $I_{DS}$ signals of the DNTT-based synaptic devices with (left) PLA and (right) PAN gate insulators exposed to light pulses. (a)–(b) [70] John Wiley & Sons. © 2017 The Authors. Published by WILEY-VCH Verlag GmbH & Co. KGaA, Weinheim. (c) Schematic of the operating principles of PEI—(left) and PAA—(right) based devices during electro-setting/resetting. Reproduced from [71] with permission from the Royal Society of Chemistry. (d) Effect of polymer molecular weight on CF diffusion in the polymer-based memristor. (e) Device structure of the artificial synapse with two polymer media (computation and memory media). (d)–(e) Reproduced from [72]. Copyright (2020) American Chemical Society.

the effect of other functional groups on the synaptic properties of organic synaptic transistors, [2,-b:2′,3′-f]-thieno[3,2-b]thiophene (DNTT)-based synaptic devices were fabricated using different polymer dielectrics of polylactide (PLA) and polyacrylonitrile (PAN) (figure 3(a)) [70]. PLA and PAN have carboxyl and nitrile groups, respectively, and the dipole moment of each functional group is 1.6 D and 3.9 D, respectively. As the dipole moments of the functional groups increase, the photoluminescence intensity also increases in the wavelength range of 520–580 nm. This wavelength range is assigned to trapped excitons; therefore, the polymer with a higher polarity of functional groups (PAN) has stronger interfacial charge-trapping characteristics. Organic synapses with PLA dielectric exhibit a relatively small dipole moment. As a result, the photogenerated charges are trapped relatively weakly. In contrast, synaptic devices with PAN dielectric exhibit a large dipole moment. Consequently, photogenerated charge carriers are continuingly trapped in the interface due to the strong interfacial effect. When a light spike is applied, photogenerated charge carriers are trapped in the OSC/dielectric interface. Due to the higher dipole moment of PAN, the device using PAN indicated a longer decay time of excitatory postsynaptic current (EPSC) (figure 3(b)). This result shows that the high dipole moment of a functional group can lead to long-term charge trapping, providing an understanding of the interfacial effect of the OSC/insulator layer on synaptic characteristics.

In addition to the gate insulating layer, the polymeric insulators can be used as a charge trapping layer in synaptic transistors [73]. When the polymer layer is inserted between the semiconducting and gate insulating layer, it is directly involved in the charge trapping process of the synaptic transistor, affecting the decay time. To increase the decay time, which is crucial in the field of non-volatile memory, a method of adjusting the dihedral angle of the side chain in polymer has been proposed. The steric hindrance caused by the bulky side chain tilts the dihedral angle of the carbon chain of the polymer, inducing charge trapping [74, 75]. In

addition, using a long side chain, such as alkyl chain, isolates the trapping sites from the semiconducting/insulating layer, preventing the loss of the trapped charges and resulting in a longer retention time [76].

In two-terminal devices, the functional groups of an insulating polymer also attribute to synaptic characteristics. Poly(ethyleneimine) (PEI) and poly(acrylic acid) (PAA) were doped with $Ca^{2+}$, and each was used as an insulator layer in memristors [71]. While PEI has a cation ($-NH_3^+$), PAA has an anion ($-COO^-$). Due to the different charge types of functional groups of insulator layer, each $Ca^{2+}$-doped memristor exhibits different properties. In a PEI-$Ca^{2+}$ device, when a negative bias is applied to the TE, the cations ($-NH_3^+$) of PEI move to the TE, thereby hindering $Ca^{2+}$ to contact at the TE. On the contrary, when a positive bias is applied to the TE, the cations ($-NH_3^+$) of PEI move to the BE, thereby hindering $Ca^{2+}$ to contact at the BE. Consequently, PEI dielectric acts as a blocking layer, preventing the formation of filament-like $Ca^{2+}$ flux (figure 3(c), left). In a PAA-$Ca^{2+}$ device, when a negative bias is applied to the TE, the anions ($-COO^-$) of PAA move to the BE, forming a mutual attraction with $Ca^{2+}$ and facilitating the construction of a filament-like $Ca^{2+}$ (figure 3(c), right). Consequently, due to filament-like $Ca^{2+}$ flux induced by the negatively charged anions ($-COO^-$) of PAA, only the PAA-based memristor exhibited stable and nonvolatile synaptic characteristics.

In addition to the effect of the functional groups of insulating polymers, controlling the molecular weight of polymers is also useful for modulating synaptic functions. In three-terminal devices, photonic synaptic transistors were fabricated using poly(N-vinylcarbazole) (PVK) electrets with two different molecular weights (low-$M_W$ PVK = 90 000 g mol$^{-1}$ and high-$M_W$ PVK = 1100 000 g mol$^{-1}$, $M_w$= weight-average molecular weight) [77]. While both high-$M_W$ PVK- and low-$M_W$ PVK-based synaptic transistors exhibit similar grain size and roughness, the low-$M_W$ PVK-based devices exhibited a larger free volume and lower dielectric constant compared to high-$M_W$ PVK-based devices. A large free volume can act as a charge-trapping site, and a low dielectric constant induces charge carriers to tunnel into the PVK layer. Therefore, when light spikes are applied, photogenerated charge carriers are trapped at the OSC/insulating layer interface. Due to the large free volume and tunnelling effect of the low-$M_W$ PVK-based synaptic transistors, it showed longer decay time of postsynaptic current compared to the high-$M_W$ PVK-based synaptic transistors.

In two-terminal devices, polymeric memristors, which used PMMA polymers with different $M_W$ as active layers, were reported [72, 78]. A low-$M_W$ polymer has a relatively large free volume, which facilitates the diffusion of metal atoms of conductive filament (CF); hence, the low-$M_W$ polymer-based memristor exhibited short relaxation time. On the contrary, the device with a high-$M_W$ polymer exhibited long relaxation time due to the facilitated CF diffusion induced by the small free volume of polymer. (Figure 3(d)). In addition, an artificial synapse with two polymer media was fabricated to emulate the STP and LTP characteristics in a single device. A low-$M_W$ polymer and a high-$M_W$ polymer were used as the computation media for STP and LTP, respectively (figure 3(e)). Using the intercellular correlation of CFs, STP and LTP were successfully emulated in one cell by modulating the interval between electrical spikes.

## 3.2. Fabrication process

Changing the fabricating conditions is one strategy for modulating the synaptic plasticity. Thermal annealing and solvent engineering have been proposed as representative methods for the precise control of synaptic plasticity. In thermal annealing, thermal energy affects the crystal orientation and molecular packing of polymer [79–81]. Meanwhile, during solution-based fabrication processes, adapting appropriate solvent is important for polymer film crystallinity. Therefore, in this section, we discuss studies that modulate synaptic plasticity through thermal annealing and solvent engineering.

### 3.2.1. Thermal annealing

Thermal annealing can be performed to improve the crystallinity of the polymer by changing the disordered polymer chains (amorphous region) to well-ordered polymer chains (crystalline region). Therefore, studies that modulate the crystallinity of semiconducting polymer and the resultant synaptic current decay time through thermal annealing were reported in the IGPST field. IGPSTs using nonannealed and annealed poly(3-hexylthiophene-2,5-diyl) P3HT semiconducting layer were fabricated [53]. The nonannealed P3HT exhibited a wide amorphous region, and the annealed P3HT showed a wide crystalline region as the arrangement of the P3HT chains was aligned. When relatively low and negative voltage spikes are applied to nonannealed P3HT, the anions of ion gel easily penetrated into the P3HT film. When the spikes disappeared, the doped anions easily diffused back to their original positions due to the large portion of amorphous regions. On the contrary, in annealed P3HT, the anions of the ion gel require a high voltage to be doped in the P3HT film due to the highly packed and well-aligned P3HT chains (crystalline region) (figure 4(a)). In addition, the interdigitated alkyl chain present in the crystalline region of P3HT can tightly bind doped
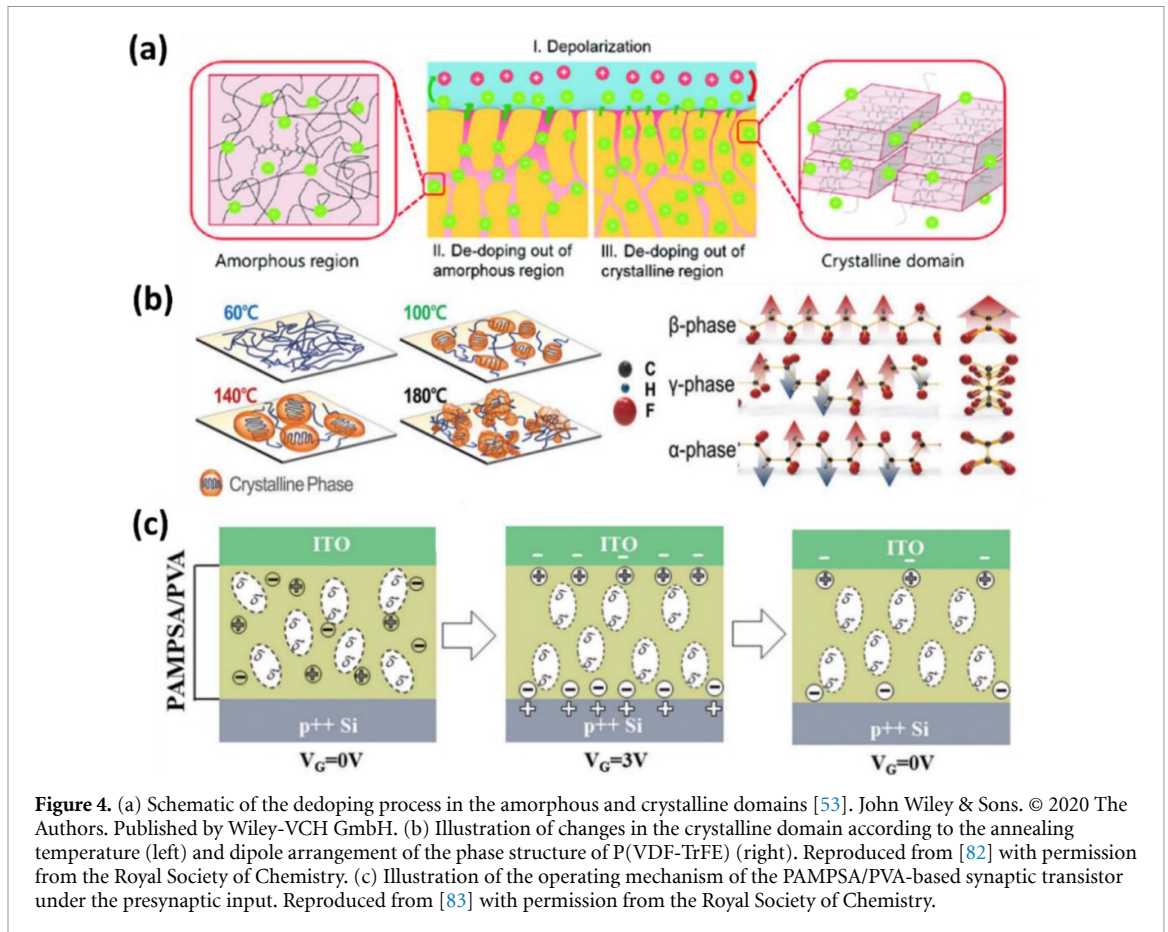
**Figure 4.** (a) Schematic of the dedoping process in the amorphous and crystalline domains [53]. John Wiley & Sons. © 2020 The Authors. Published by Wiley-VCH GmbH. (b) Illustration of changes in the crystalline domain according to the annealing temperature (left) and dipole arrangement of the phase structure of P(VDF-TrFE) (right). Reproduced from [82] with permission from the Royal Society of Chemistry. (c) Illustration of the operating mechanism of the PAMPSA/PVA-based synaptic transistor under the presynaptic input. Reproduced from [83] with permission from the Royal Society of Chemistry.

anions, preventing them from diffusing back to their original positions. As a result, thermal annealing can increase the decay time of the postsynaptic current by expanding the crystalline region. In addition to the presence or absence of thermal annealing, the effect of the thermal annealing temperature was investigated to change the synaptic characteristics. Poly(thienoisoindigo-naphthalene) (PTIIG-Np) OSC films were annealed at various temperatures (80 °C, 150 °C, 180 °C, 250 °C, and 310 °C) [52]. The OSC film exhibited low crystallinity when it was annealed at a relatively low temperature (80 °C). This temperature was not enough for the polymer to crystallize, resulting in the smallest grain size and the largest grain boundaries (GBs). These GBs become the main path through which ions move. When a gate voltage is applied, ions move near the OSC film and penetrate mainly through GBs rather than grains. When the voltage is removed, the ions easily diffuse back to their original positions through GBs. On the contrary, as the annealing temperature increases to 310 °C, the crystallinity and grain size of PTIIG-Np increases, diminishing GBs. As a result, when the same voltage is applied, due to diminished GBs, ions tend to directly penetrate into the crystalline domains rather than moving through GBs. Moreover, ions doped into crystalline domains cannot easily diffuse back to their original positions. Consequently, IGPST exhibits an increased decay time of the postsynaptic current as the annealing temperature increases. These results show that synaptic plasticity can be changed by controlling the crystallinity of the polymer through thermal annealing.

In devices based on ferroelectric mechanism, study that modulated the synaptic properties according to the annealing temperature was also reported. As discussed in section 2, when a presynaptic spike is applied, the dipoles of a gate insulator are aligned with the applied electric field. Because this alignment of dipoles is maintained even after spike is removed, the devices using ferroelectric mechanism can exhibit LTP characteristics. Moreover, because thermal energy affects the alignment of dipoles in a ferroelectric polymer, synaptic plasticity can be modulated via thermal annealing. To investigate the effect of different annealing temperatures, poly(vinylidene fluoride-trifluoroethylene) (P(VDF-TrFE)) ferroelectric copolymer annealed at different temperatures (60 °C, 140 °C, and 180 °C) was used as a gate insulator [82]. When the P(VDF-TrFE) film is annealed at the lowest temperature (60 °C), which is lower than the Curie temperature (88.3 °C), sufficient thermal energy is not provided, resulting in low ferroelectric characteristics. Meanwhile, when P(VDF-TrFE) film is annealed at 140 °C, which is above the Curie temperature (88.3 °C), the thermal energy can rearrange the orientation and position of polymer chains, forming a crystalline ferroelectric $\beta$-phase (figure 4(b), left). Furthermore, when the P(VDF-TrFE) film is annealed at 180 °C, which is above

the melting temperature (164.7 °C), $\alpha$-phase and $\gamma$-phase with nonpolar characteristics are dominantly formed, reducing the portion of $\beta$-phase (figure 4(b), right) and the resultant short decay time of the device. Thus, the device annealed at 140 °C, which is between the Curie temperature and melting temperature, showed the highest LTP characteristics due to the ferroelectric characteristics of the large $\beta$-phase domain of P(VDF-TrFE) layer.
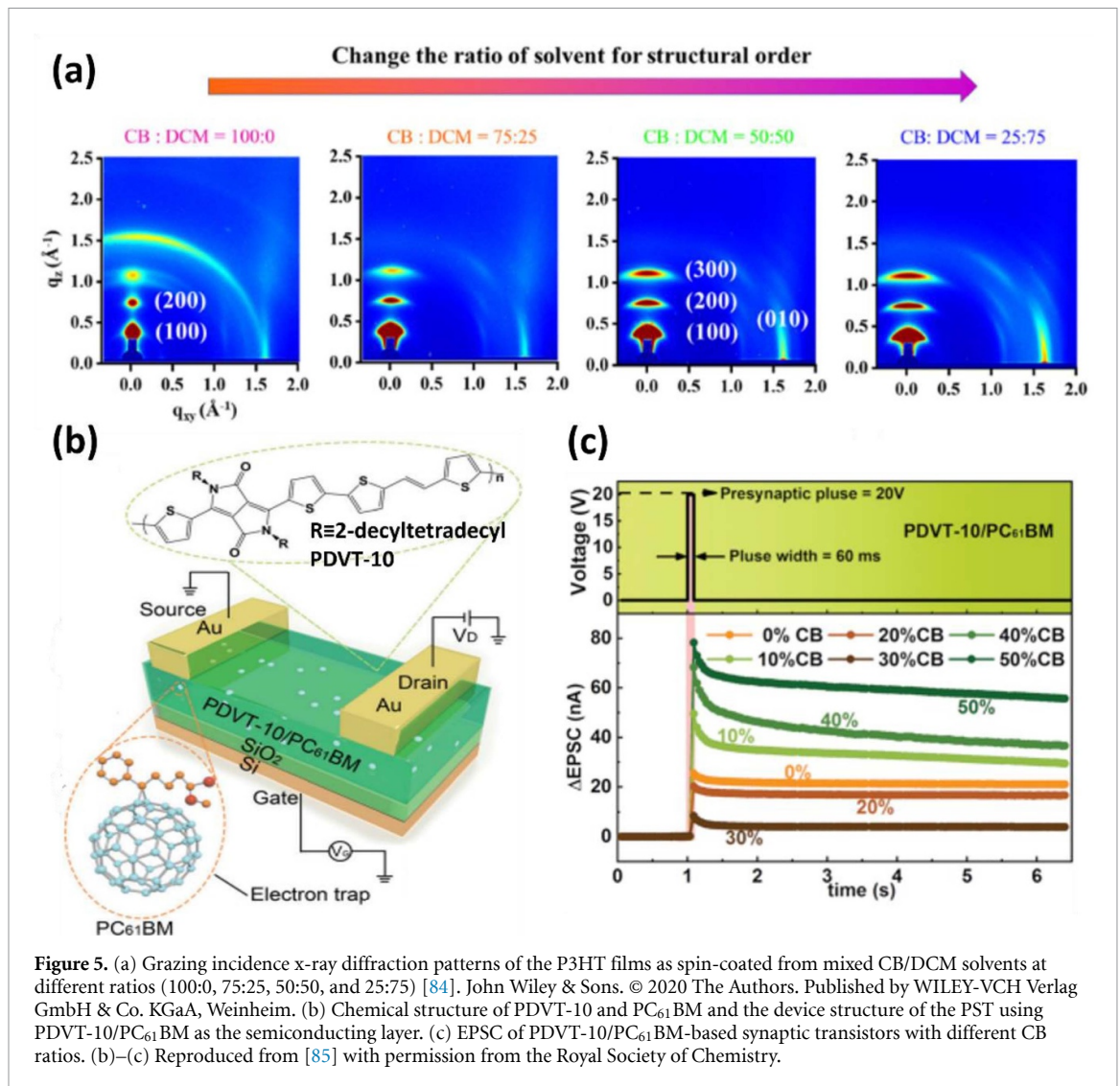
As another example of the polarization being controlled by thermal annealing, poly(2-acrylamido-2-methyl-1-propanesulfonic acid) (PAMPSA)/poly(vinyl alcohol) (PVA)-based synaptic transistors were annealed at different temperatures (110 °C, 130 °C, 150 °C and 170 °C) [83]. During the annealing process of PAMPSA/PVA-based synaptic transistors, dipoles were generated through the interaction between carbon and nitrogen molecules in the PAMPSA/PVA layer. The number of dipoles increased as the temperature increased. When a presynaptic spike was applied, the dipoles were aligned, increasing the channel conductance and maintaining the alignment of dipoles even after the voltage was removed (figure 4(c)). Consequently, the decay time of EPSC increased as the annealing temperature increased.

*3.2.2. Solvent engineering*

Solvents have shown a significant effect on the microstructure of polymers, thus modulating the synaptic properties. To investigate how adjusting the ratio of solvents in cosolvent systems affects the microstructure of the polymer film, P3HT–based IGPST was fabricated with various cosolvent ratios [chlorobenzene (CB):dichloromethane (DCM) ratios of 100:0, 75:25, 50:50, and 25:75]. A good solvent (CB) and poor solvent (DCM) were used to achieve the appropriate crystallinity of the polymer for the desired synaptic plasticity [84]. In a good solvent (CB), P3HT is completely dissolved, forming an amorphous state, whereas in a poor solvent (DCM), P3HT chains aggregate, forming highly crystalline nanowires. As DCM/CB ratio increases, the fabricated P3HT films exhibits higher crystallinity and roughness (figure 5(a)). The high crystallinity of P3HT interferes with the back diffusion of ions trapped in the ion-gel/P3HT interface or injected in P3HT, increasing the decay time of the postsynaptic current. On the contrary, the roughness of the polymer acts as a counteractive factor to current, i.e. the high roughness film caused the reduction of the postsynaptic current. Therefore, a balance between the film crystallinity and roughness is important. Increasing the proportion of DCM from 0% to 50% leads to enhanced crystallinity, thereby increasing the decay time of the postsynaptic current. However, a high proportion of DCM (CB:DCM = 25:75 and 0:100) leads to increased roughness, thereby decreasing the decay time. As a result, due to the conflicting effects between film crystallinity and roughness, the longest decay time of the postsynaptic current was obtained at a CB:DCM ratio of 50:50.

Furthermore, the boiling point of a solvent can influence the decay time of synaptic current. The ratio of the high boiling point of CB and the low boiling point of chloroform (CF) was adjusted to investigate how the boiling point of a solvent affects the polymer film formation. A poly[2,5-bis(alkyl)pyrrolo[3,4-c]pyrrolo-1,4(2 H,5 H)-dione-alt-5,5-di(thiophene-2-yl)-2,2-(E)-2-(2-(thiophen-2-yl)-vinyl)thiophene] (PDVT-10)/[6,6]-phenyl $C_{61}$ butyric acid methyl ester ($PC_{61}BM$) film was used (figure 5(b)) as the bulk heterojunction semiconducting layer [85]. PDVT-10 and $PC_{61}BM$ were prepared by dissolving them in a CB and CF cosolvent. The PDVT-10/$PC_{61}BM$ mixture exhibited different synaptic behaviours depending on the cosolvent ratio. In a pure low boiling point of the CF solvent (0% CB), $PC_{61}BM$ was uniformly dispersed in PDVT-10, enhancing the probability of the electron trap in $PC_{61}BM$ and thus increasing the decay time of the postsynaptic current. As the high boiling point of the CB ratio increased by up to 30%, the CB solvent provided more time for the phase separation of PDVT-10/$PC_{61}BM$ to occur, causing $PC_{61}BM$ to aggregate. Therefore, a continuous pathway of aggregated $PC_{61}BM$ was constructed between the source and drain electrodes. This pathway facilitated the release of trapped electron, reducing the decay time of the postsynaptic current. However, when the CB ratio increased to 50%, a $PC_{61}BM$ aggregation was enhanced and the continuous $PC_{61}BM$ pathway between the source and drain electrodes failed to form. Thus, the device having 50% CB showed the longest decay time of the postsynaptic current (figure 5(c)).

Throughout this section, we have reviewed various studies that modulated synaptic plasticity through thermal annealing and solvent engineering. These fabrication processes are important for modulating the microstructures of semiconducting and insulating polymers, such as packing of polymer and alignment of dipoles, thereby affecting synaptic plasticity. In addition to the methods introduced above, there are studies that changed synaptic plasticity by introducing a simple process. For example, an ultraviolet light exposure process was adopted to cross-link polymers and successfully implement STP and LTP using the cross-linked polymer [86]. Additionally, a doping process can be applied to increase the retention time in the field of nonvolatile memory [87]. For example, the zeolite imidazolate framework-8 (ZIF-8) nanoparticles are doped in the polyvinylpyrrolidone (PVP) polymer matrix, which is an active layer located between the Ag and ITO electrodes. Due to the larger pore size of ZIF-8 (0.34 nm) than $Ag^+$ (0.23 nm), the ZIF-8 facilitates the

**Figure 5.** (a) Grazing incidence x-ray diffraction patterns of the P3HT films as spin-coated from mixed CB/DCM solvents at different ratios (100:0, 75:25, 50:50, and 25:75) [84]. John Wiley & Sons. © 2020 The Authors. Published by WILEY-VCH Verlag GmbH & Co. KGaA, Weinheim. (b) Chemical structure of PDVT-10 and $PC_{61}BM$ and the device structure of the PST using PDVT-10/$PC_{61}BM$ as the semiconducting layer. (c) EPSC of PDVT-10/$PC_{61}BM$-based synaptic transistors with different CB ratios. (b)–(c) Reproduced from [85] with permission from the Royal Society of Chemistry.

penetration of $Ag^+$ from TE to BE to form the CFs under the voltage bias. Furthermore, because of the ionic-trapping effect of ZIF-8, Ag metal is trapped at the interface between PVP and ZIF-8, which improves the retention time [88]. Thus, combining various methods, such as changing conditions like thermal annealing temperature and the cosolvent ratio can achieve the desired synaptic properties, which is required in a wide range of neuromorphic applications, including bioelectronics and neuromorphic computing.

# 4. Application

Herein, we reviewed various synaptic devices that modulated synaptic plasticity using different types of polymers and fabrication processes. Using these devices, many studies were conducted to demonstrate neuromorphic application. The purpose of a neuromorphic device is to mimic the biological brain and peripheral nerves, which has the ability to learn and memorize, and the biological nervous system, which can sense and process external stimuli. To emulate abilities of the brain, synaptic devices have been reported to demonstrate logic and recognize patterns and images. Meanwhile, to replicate nervous systems, various synaptic devices that integrate sensing/motor functions are reported. In this section, we review previous studies discussing the applications of polymer-based synaptic devices.

### 4.1. Neuromorphic computing
The polymer structure can be modified in several ways to adjust the synaptic plasticity from STP to LTP. This is essential for the construction of neural networks for neuromorphic computing and laying the foundation for the development of various applications beyond neuromorphic computing. For neuromorphic
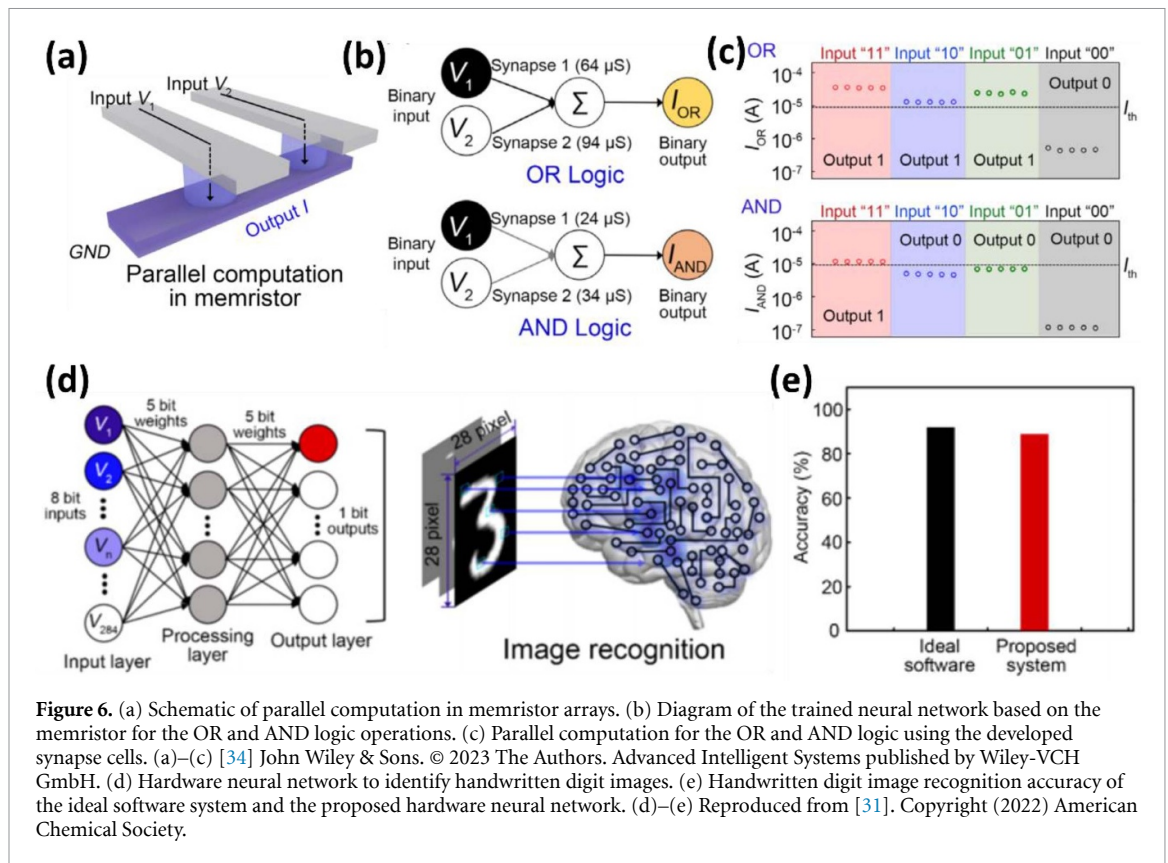
**Figure 6.** (a) Schematic of parallel computation in memristor arrays. (b) Diagram of the trained neural network based on the memristor for the OR and AND logic operations. (c) Parallel computation for the OR and AND logic using the developed synapse cells. (a)–(c) [34] John Wiley & Sons. © 2023 The Authors. Advanced Intelligent Systems published by Wiley-VCH GmbH. (d) Hardware neural network to identify handwritten digit images. (e) Handwritten digit image recognition accuracy of the ideal software system and the proposed hardware neural network. (d)–(e) Reproduced from [31]. Copyright (2022) American Chemical Society.

computing, hardware neural networks were implemented using synaptic devices [33]. First, a memristor array was designed for parallel computing (figure 6(a)) [31, 34]. Multiple memristors cells, which act as artificial synapses, were trained on OR and AND logic (figure 6(b)). In this structure, two synapses connect two input neurons and one output neuron. A different voltage was applied to each input node, and a current corresponding to OR and AND was output through the output node. The input signals '1' and '0' corresponded to reading voltages of 0.2 and 0.002 V, respectively. At this time, the output was determined as '1' when the output current was 9 $\mu$A or more and '0' when the output current was lower than 9 $\mu$A (figure 6(c)). These systems showed reliable computing results for OR and AND logic and demonstrated high capability for parallel computing. In addition, the use of polymer as the insulator layer of memristor not only showed stable operation in the bending test but also consumed low energy (~fJ level).

Furthermore, to realize an actual intelligent system, a complex neural network was designed, and its performance was evaluated through pattern image recognition. This neural network was designed to classify handwritten digit images based on datasets from the Modified National Institute of Standards and Technology (MNIST). In the simulation, the MNIST dataset composed of 60 000 and 10 000 images for learning and for classifying tests, respectively. Handwritten digit images were classified through 28 × 28 pixels. The neural network consists of an input layer, consisting of 784 neurons, for digit image recognition, a processing layer with 32 neurons, and an output layer with 10 neurons for input digit classification (figure 6(d)). Images recognized through input layer were calculated through the conductance of synapses and derived as output results. Proposed neural network based on the memristors consisting of the polymer insulating layer reliably recognized handwritten digits with an accuracy of approximately 90%, which is close to software system with 92% accuracy (figure 6(e)). The proposed neural network also showed an 85% accuracy in simulation using Fashion MNIST datasets and were successfully applied [32]. These results suggest that polymer-based memristors that can implement various synaptic characteristics can be applied to neuromorphic systems, such as hardware neural networks and AI.

### 4.2. Artificial synaptic devices with sensing functions
Artificial synaptic devices with sensing functions that mimic biological sensory abilities for touch, chemicals, and light were reported using polymers that can react to external stimuli through various mechanisms, such
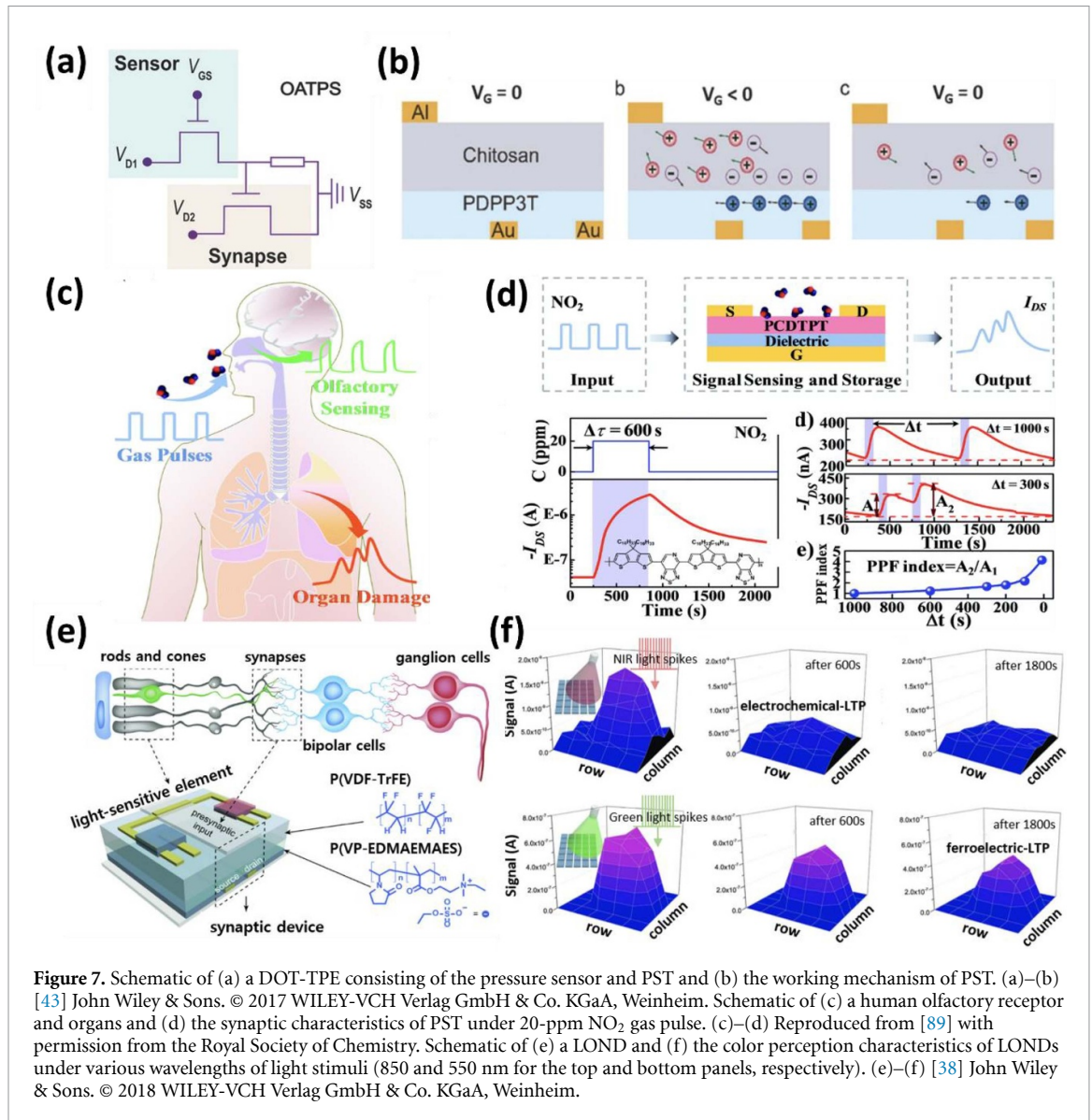
**Figure 7.** Schematic of (a) a DOT-TPE consisting of the pressure sensor and PST and (b) the working mechanism of PST. (a)–(b) [43] John Wiley & Sons. © 2017 WILEY-VCH Verlag GmbH & Co. KGaA, Weinheim. Schematic of (c) a human olfactory receptor and organs and (d) the synaptic characteristics of PST under 20-ppm $NO_2$ gas pulse. (c)–(d) Reproduced from [89] with permission from the Royal Society of Chemistry. Schematic of (e) a LOND and (f) the color perception characteristics of LONDs under various wavelengths of light stimuli (850 and 550 nm for the top and bottom panels, respectively). (e)–(f) [38] John Wiley & Sons. © 2018 WILEY-VCH Verlag GmbH & Co. KGaA, Weinheim.

as charge trapping and ferroelectricity. A dual-organic-transistor-based tactile-perception element (DOT-TPE) was reported in an artificial tactile-perception system [43]. In the DOT-TPE, the pressure-sensitive organic field-effect transistor (OFET) and PST were connected in serial (figure 7(a)). In the PST, poly(diketopyrrolopyrrole-terthiophene) (PDPP3T) and chitosan were used for an organic semiconducting layer and gate insulating layer, respectively. When a dynamic external pressure was applied to the DOT-TPE, the gate of the pressure sensor deformed and the capacitance of the dielectric layer increased, leading to a decrease in the resistance of the pressure-sensing device. Therefore, the pressure stimuli were transferred to the gate of the PST. As the stimuli were applied, mobile protons in dielectric migrated toward the gate electrode and electrons moved to the semiconductor/dielectric interface. Therefore, the induced electrons near the semiconductor/dielectric interface attracted holes in the PDPP3T channel layer, increasing the postsynaptic current level (figure 7(b)). Due to the synaptic properties of the DOT-TPE, the output current can be modulated not only based on the intensity but also the frequency, duration, and number of pressures. Based on the information processes by the DOT-TPE, the DOT-TPE showed tactile-perception ability.

To imitate the human olfactory perception, a conformable artificial memory system that can sense hazardous gas leakage (e.g. $NO_2$) was constructed based on PST. This PST was fabricated based on flexible PVA substrate, and poly[4-(4,4-dihexadecyl-4H-cyclopenta[1,2-b:5,4-b′]dithiophen-2-yl)-alt-[1,2,5] thiadiazolo[3,4-c]pyridine] (PCDTPT) was used as the semiconducting layer [89]. When $NO_2$ gas was injected into the PCDTPT semiconducting layer, $NO_2$ molecules were captured and served as an effective

electron trapping site. Thus, holes accumulated in the semiconducting layer, leading to the improvement in the current level. When a $NO_2$ gas pulse was removed, $NO_2$ molecules could not be dedoped instantly. Thus, an increased current showed slow decay time. Consequently, this artificial PST exhibited synaptic properties and capability to sense $NO_2$ gas (figures 7(c) and (d)).

In artificial visual perception system, a light-triggered organic neuromorphic device (LOND) was fabricated using ferroelectric/electrochemical modulated synapses to imitate retinal functions (figure 7(e)) [38]. In this PST, nonvolatile LTP characteristics were emulated by introducing a ferroelectric polymer gate dielectric P(VDF-TrFE). This synapse exploited both electrochemical doping and ferroelectric mechanism. Consequently, switching between electrochemical and ferroelectric modes can be achieved by varying the gate voltage amplitude, thus demonstrating three types of synaptic characteristics (STP, electrochemical LTP, and ferroelectric LTP). These characteristics can then be used to demonstrate the organic visual perception system and color recognition ability of LOND. When light stimuli are applied, LOND converts light intensity and frequency information into tunable EPSC signal. Considering the color recognition ability of LOND, electrochemical LTP and ferroelectric LTP appeared under 850-nm light (near-infrared light) and 550 nm light (green light), respectively (figure 7(f)).

### 4.3. Artificial nerves for neuroprostheses

In addition to mimicking biological sensory abilities, constructing biohybrid neuromorphic systems that integrate artificial and biological nervous systems is important to achieve further advanced neuromorphic applications, such as sensorimotor nervetronics and neuroprostheses [20, 90, 91]. These systems perform the task of detecting and processing physiological signals by mimicking the biological nervous system. Therefore, artificial nervous systems for biohybrid neuromorphic systems should be constructed with biocompatible characteristics and mechanical properties similar to those of living organisms. Polymers are in the spotlight for this purpose because of their superior biocompatibility and mechanical flexibility compared to other materials (e.g. inorganic materials). Biocompatible polymers are less toxic to cells and can be modified to have hydrophilic surfaces, enabling them to adhere well to the hydrophilic cells [92–95]. Moreover, the mechanical flexibility of polymers minimizes mechanical mismatch with biological tissues because their Young's moduli are close to those the biological tissues, preventing inflammation and detachment [20, 96]. Consequently, polymer-based synaptic devices integrate smoothly with biohybrid neuromorphic systems without causing damage and can operate energy-efficiently without the need for bulky and rigid external computing units.

For example, an artificial afferent nerve using polymer synaptic devices was reported. This artificial afferent nerve consists of a resistive pressure sensor, organic ring oscillators, and synaptic transistors [97]. In an artificial nervous system, artificial mechanoreceptors that detect pressure stimuli are connected to an artificial nerve fiber (a ring oscillator), changing tactile stimuli into voltage spikes (figure 8(a)). These voltage spikes of artificial nerve fibers are transferred to synaptic transistors, leading to postsynaptic current. Moreover, synaptic transistors were connected to a biological motor nerve in a detached cockroach leg (figure 8(b)). This combination of artificial afferent nerve and biological motor nerve demonstrates a hybrid reflex arc. When the external pressure information from the pressure sensor is transported to the motor nerve in the cockroach leg, the muscle in the leg is actuated according to the external pressure information. These behaviours of the artificial afferent nerve contribute to its potential to be applied in neurorobots and neuroprostheses. In addition to this potential to neuromorphic applications, an artificial afferent nerve can recognize the movement direction of an object, and a pixel array of artificial afferent nerves is used to identify Braille characters.

In addition, a recent study reported a stretchable neuromorphic efferent nerve (SNEN) using a stretchable polymeric nanowire synaptic transistor (figure 8(c)) [15]. This SNEN was attached to the muscle of mouse's legs. The EPSC value increased when leg extension occurred. However, with excessive leg extension, the voltage divider circuit increased the resistance of the strain sensor. Thus, EPSC can be downregulated, limiting the potentiation of the EPSC level of the PST. This negative feedback mechanism prevented damage in the muscle induced by the excessive extension of the muscle. Furthermore, even after 1,000 times of repeated stretching to 100% strain, the synaptic transistor maintained stable electrical characteristics. These stable mechanical characteristics and feedback processes demonstrate the ability of SNEN. SNEN can bypass the spinal injury and inspire further development of neuromorphic devices.
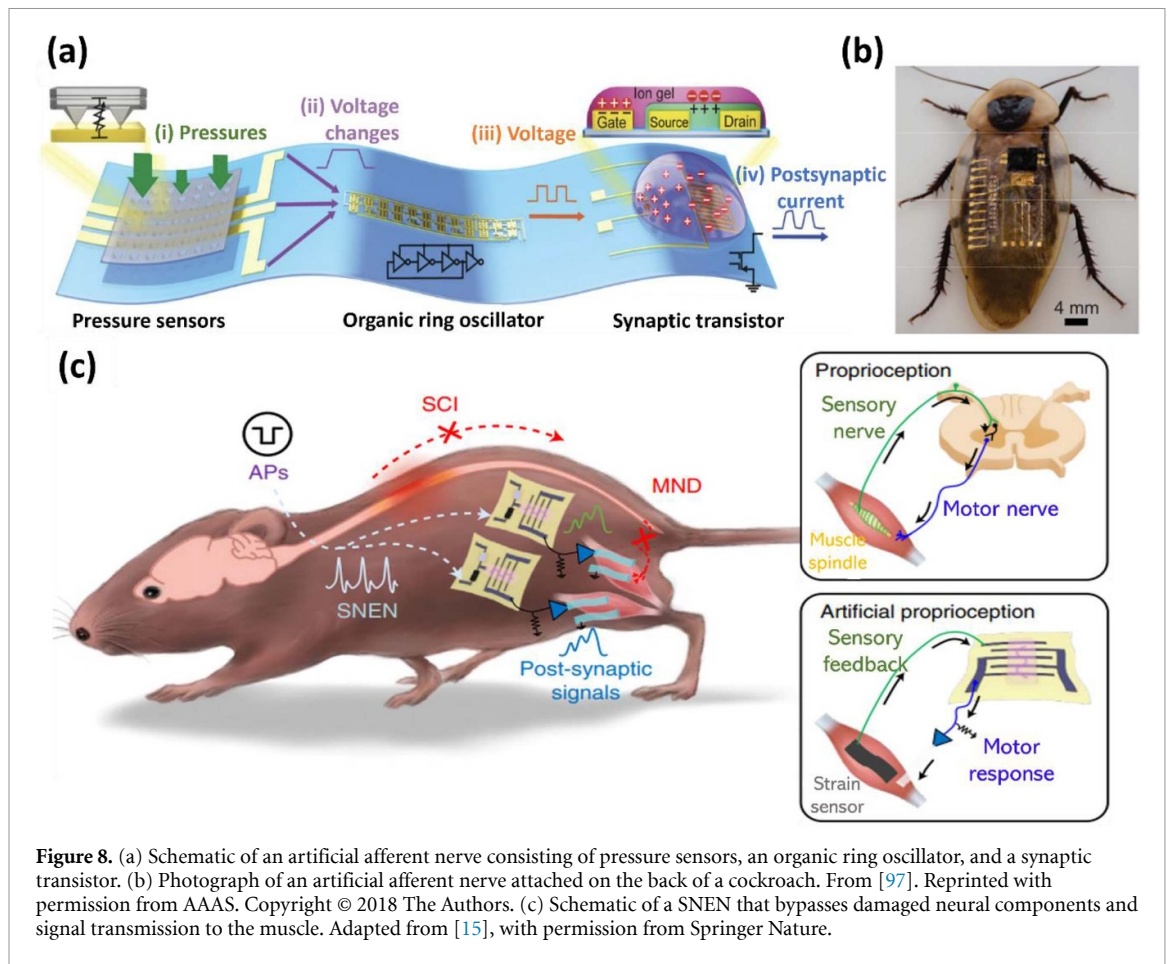
**Figure 8.** (a) Schematic of an artificial afferent nerve consisting of pressure sensors, an organic ring oscillator, and a synaptic transistor. (b) Photograph of an artificial afferent nerve attached on the back of a cockroach. From [97]. Reprinted with permission from AAAS. Copyright © 2018 The Authors. (c) Schematic of a SNEN that bypasses damaged neural components and signal transmission to the muscle. Adapted from [15], with permission from Springer Nature.

## 5. Conclusion

We reviewed the recent progress of polymer-based synaptic devices, including the operating mechanisms, and discussed how to implement diverse decay time in polymeric synaptic devices. More specifically, in polymer-based synaptic devices, we proposed the changes in the molecular structure and fabrication processes as strategies to demonstrate various synaptic characteristics. The type or length of the side chain of the polymer backbone was modulated for the molecular engineering of a polymer semiconducting layer. For insulating materials, using different types of functional groups or decreasing the molecular weight enhanced the charge trapping and construction of filament, resulting in successful implementation of various synaptic functions. Meanwhile, adjusting the fabrication process was investigated to modulate the synaptic plasticity over a wide timescale. For the thermal annealing of the polymer film, improving the crystallinity of the polymer through the ordering of polymer chains can be achieved by controlling the thermal annealing temperature. The improved polymer crystallinity induced relatively long decay time. In addition, in solvent engineering, controlling of the solvent ratio in cosolvents was investigated. Due to the different characteristics of the solvents, such as solubility and boiling point, modulating the solvent ratio in cosolvents also affected synaptic plasticity by changing the microstructure of the polymer film. Based on the polymer-based synaptic devices, applications such as neuromorphic computing, artificial synaptic devices with sensing functions, and artificial nerves for neuroprostheses that imitates biological nervous systems have been introduced.

These polymer-based synaptic devices can implement a wide range of decay time (STP to LTP), mimicking the learning and memory functions of the biological nervous system. In addition, polymers are particularly suitable for practical applications due to their light-weight, flexible, and biocompatible properties. With increasing demand for health monitoring and IoT, research on wearable electronics, smart sensors, and bioelectronics is growing. Polymers can adhere well to the curved surface of the human body due to their excellent flexibility, essential for wearable electronics and smart sensors that collect physiological signals from the biological nervous system. Moreover, biocompatible polymers do not trigger an immune response, making them suitable for integration into the human body as bioelectronics.

While adjusting decay time has been a primary focus among synaptic properties, various synaptic characteristics should be considered for practical application. Studies are needed to implement biorealistic

synaptic properties in the polymer-based synaptic device by altering material or device structures. For example, linearity in potentiation/depression, which ensures a uniform conductance change, is crucial for learning accuracy in artificial neural network and neuromorphic computing [73, 98]. Improving linearity can be achieved by increasing crystallinity through annealing the polymer semiconducting layer, suppressing sudden ion diffusion [52]. Another approach involves balancing the carrier trapping by inserting a floating or tunneling layer in a polymer-based synaptic transistor [99, 100].

Real-world application of polymer-based neuromorphic devices requires environmental stability. Typically, polymers are sensitive to environmental factors such as humidity, oxygen, and high temperature, which can lead to degradation of device performance. Specifically, integrated electronic circuits require high temperature stability for long-term operation. To overcome these limitations, approaches such as encapsulation techniques can be considered. Additionally, compact-sized device and high-density integration are necessary for processing a large amount of complex information, a, but volume reduction remains a challenge. Proposed solutions include memristive crossbar array and multi-gated transistor structures [101, 102]. Overcoming these limitations will enable polymer-based synaptic devices to surpass existing neuromorphic computing constraints and be applied in advanced healthcare and biomedical applications requiring long-term and environmental stability.

## Data availability statement

No new data were created or analysed in this study.

## Acknowledgments

## ORCID iDs

Hea-Lim Park ⬤ https://orcid.org/0000-0001-8370-7068
Tae-Woo Lee ⬤ https://orcid.org/0000-0002-6449-6725

## References

[1] Park H-L and Lee T-W 2021 Organic and perovskite memristors for neuromorphic computing *Org. Electron.* **98** 106301
[2] Hu M *et al* 2018 Memristor-based analog computation and neural network classification with a dot product engine *Adv. Mater.* **30** 1705914
[3] Park H, Lee Y, Kim N, Seo D, Go G and Lee T 2020 Flexible neuromorphic electronics for computing, soft robotics, and neuroprosthetics *Adv. Mater.* **32** 1903558
[4] Lee Y, Park H-L, Kim Y and Lee T-W 2021 Organic electronic synapses with low energy consumption *Joule* **5** 794–810
[5] Raeis-Hosseini N, Park Y and Lee J-S 2018 Flexible artificial synaptic devices based on collagen from fish protein with spike-timing-dependent plasticity *Adv. Funct. Mater.* **28** 1800553
[6] Kim S E, Kim M-H, Jang J, Kim H, Kim S, Jang J, Bae J-H, Kang I M and Lee S-H 2022 Systematic engineering of metal ion injection in memristors for complex neuromorphic computing with high energy efficiency *Adv. Intell. Syst.* **4** 2200110
[7] Ro J-S, An H-M and Park H-L 2023 Electrolyte-gated synaptic transistors for brain-inspired computing *Jpn. J. Appl. Phys.* **62** SE0801
[8] Park H-L, Jun J, Kim M-H and Lee S-H 2022 Introduction of helical photonic crystal insulator in organic phototransistor for enhancing selective color absorption *Org. Electron.* **100** 106385
[9] An H-M, Jang H, Kim H, Lee S-D, Lee S-H and Park H-L 2023 Engineered current path of vertical organic phototransistors for smart optoelectronic applications *J. Mater. Chem.* C **11** 14580–8
[10] Abraham W C and Robins A 2005 Memory retention—the synaptic stability versus plasticity dilemma *Trends Neurosci.* **28** 73–78
[11] Zhang C *et al* 2016 Synaptic plasticity and learning behaviours in flexible artificial synapse based on polymer/viologen system *J. Mater. Chem.* C **4** 3217–23
[12] Guo T, Ge J, Sun B, Pan K, Pan Z, Wei L, Yan Y, Zhou Y N and Wu Y A 2022 Soft biomaterials based flexible artificial synapse for neuromorphic computing *Adv. Electron Mater.* **8** 2200449
[13] Liu R, Yang W, Xu W, Deng J, Ding C, Guo Y, Zheng L, Sun J and Li M 2022 Impact of chemical design on the molecular orientation of conjugated donor-acceptor polymers for field-effect transistors *ACS Appl. Polym. Mater.* **4** 2233–50
[14] He Z, Zhang Z, Asare-Yeboah K and Bi S 2023 Binary solvent engineering for small-molecular organic semiconductor crystallization *Mater. Adv.* **4** 769–86
[15] Lee Y *et al* 2023 A low-power stretchable neuromorphic nerve with proprioceptive feedback *Nat. Biomed. Eng.* **7** 511–9
[16] Hormuzdi S G, Filippov M A, Mitropoulou G, Monyer H and Bruzzone R 2004 Electrical synapses: a dynamic signaling system that shapes the activity of neuronal networks *Biochim. Biophys. Acta Biomembr.* **1662** 113–37
[17] Faber D S and Pereda A E 2018 Two forms of electrical transmission between neurons *Front. Mol. Neurosci.* **11** 427
[18] Pereda A E 2014 Electrical synapses and their functional interactions with chemical synapses *Nat. Rev. Neurosci.* **15** 250–63

[19] Lewis R, Asplin K E, Bruce G, Dart C, Mobasheri A and Barrett-Jolley R 2011 The role of the membrane potential in chondrocyte volume regulation *J. Cell Physiol.* **226** 2979–86

[20] Kim K N, Sung M J, Park H L and Lee T W 2022 Organic synaptic transistors for bio-hybrid neuromorphic electronics *Adv. Electron. Mater.* **8** 2100935

[21] Kakegawa W and Yuzaki M 2005 A mechanism underlying AMPA receptor trafficking during cerebellar long-term potentiation *Proc. Natl Acad. Sci.* **102** 17846–51

[22] Riedemann T, Patchev A V, Cho K and Fx Almeida O 2010 Corticosteroids: way upstream Mol. Brain 3

[23] Shen J X, Shang D S, Chai Y S, Wang S G, Shen B G and Sun Y 2018 Mimicking synaptic plasticity and neural network using memtranstors *Adv. Mater.* **30** 1706717

[24] Gkoupidenis P, Schaefer N, Garlan B and Malliaras G G 2015 Neuromorphic functions in PEDOT:PSS organic electrochemical transistors *Adv. Mater.* **27** 7176–80

[25] Liu Y H, Zhu L Q, Feng P, Shi Y and Wan Q 2015 Freestanding artificial synapses based on laterally proton-coupled transistors on chitosan membranes *Adv. Mater.* **27** 5599–604

[26] Xu W, Min S Y, Hwang H and Lee T W 2016 Organic core-sheath nanowire artificial synapses with femtojoule energy consumption *Sci. Adv.* **2** e1501326

[27] Kang D H, Jun H G, Ryoo K C, Jeong H and Sohn H 2015 Emulation of spike-timing dependent plasticity in nano-scale phase change memory *Neurocomputing* **155** 153–8

[28] Kim S I *et al* 2019 Dimensionality dependent plasticity in halide perovskite artificial synapses for neuromorphic computing *Adv. Electron Mater.* **5** 1900008

[29] Chen S, Lou Z, Chen D and Shen G 2018 An artificial flexible visual memory system based on an UV-motivated memristor *Adv. Mater.* **30** 1705400

[30] Park H L, Kim M H and Lee S H 2020 Introduction of interfacial load polymeric layer to organic flexible memristor for regulating conductive filament growth *Adv. Electron Mater.* **6** 2000582

[31] Park M W, Kim D Y, An U, Jang J, Bae J H, Kang I M and Lee S H 2022 Organizing reliable polymer electrode lines in flexible neural networks via coffee ring-free micromolding in capillaries *ACS Appl. Mater. Interfaces* **14** 46819–26

[32] Kim M H, Park H L, Kim M H, Jang J, Bae J H, Kang I M and Lee S H 2021 Fluoropolymer-based organic memristor with multifunctionality for flexible neural network system *npj Flex. Electron.* **5** 34

[33] Kim H, Kim M, Lee A, Park H L, Jang J, Bae J H, Kang I M, Kim E S and Lee S H 2023 Organic memristor-based flexible neural networks with bio-realistic synaptic plasticity for complex combinatorial optimization *Adv. Sci.* **10** 2300659

[34] Oh S, Kim H, Kim S E, Kim M H, Park H L and Lee S H 2023 Biodegradable and flexible polymer-based memristor possessing optimized synaptic plasticity for eco-friendly wearable neural networks with high energy efficiency *Adv. Intell. Syst.* **5** 2200272

[35] Zhao X *et al* 2017 Confining cation injection to enhance CBRAM performance by nanopore graphene layer *Small* **13** 1603948

[36] Lee S-H, Park H-L, Kim M-H, Kang S and Lee S-D 2019 Interfacial triggering of conductive filament growth in organic flexible memristor for high reliability and uniformity *ACS Appl. Mater. Interfaces* **11** 30108–15

[37] Lee Y R, Trung T Q, Hwang B U and Lee N E 2020 A flexible artificial intrinsic-synaptic tactile sensory organ *Nat. Commun.* **11** 2753

[38] Wang H *et al* 2018 A ferroelectric/electrochemical modulated organic synapse for ultraflexible, artificial visual-perception system *Adv. Mater.* **30** 1803961

[39] Lee H R, Lee D and Oh J H 2021 A hippocampus-inspired dual-gated organic artificial synapse for simultaneous sensing of a neurotransmitter and light *Adv. Mater.* **33** 2100119

[40] Yan M *et al* 2021 Ferroelectric synaptic transistor network for associative memory *Adv. Electron. Mater.* **7** 2001276

[41] Xu Q, Chen J, Li Y, Qiu J, Liu X, Cao J, Chen Y, Liu M and Wang M 2024 Fully printed dual-gate organic electrochemical synaptic transistor with neurotransmitter-mediated plasticity *IEEE Electron Device Lett.* **45** 104–7

[42] Liu X, Sun C, Guo Z, Zhang Y, Zhang Z, Shang J, Zhong Z, Zhu X, Yu X and Li R-W 2022 A flexible dual-gate hetero-synaptic transistor for spatiotemporal information processing *Nanoscale Adv.* **4** 2412–9

[43] Zang Y, Shen H, Huang D, Di C A and Zhu D 2017 A dual-organic-transistor-based tactile-perception system with signal-processing functionality *Adv. Mater.* **29** 1606088

[44] Deng Z, Zhou B, Xu Y, Jin C, Liu W, Liu B, Sun J and Yang J 2022 Recent progresses of organic photonic synaptic transistors *Flex. Print. Electron.* **7** 024002

[45] Park H L, Kim H, Lim D, Zhou H, Kim Y H, Lee Y, Park S and Lee T W 2020 Retina-inspired carbon nitride-based photonic synapses for selective detection of UV light *Adv. Mater.* **32** 1906899

[46] Zhao Y, Wang W, He Z, Peng B, Di C A and Li H 2023 High-performance and multifunctional organic field-effect transistors *Chin. Chem. Lett.* **34** 108094

[47] Ko G M, Kang Y G, Jeong U C, Lee T W and Park H L 2023 Polymeric gate insulators to induce synaptic photoresponse of organic transistors *J. Korean Phys. Soc.* **83** 320–7

[48] Park E *et al* 2020 A 2D material-based floating gate device with linear synaptic weight update *Nanoscale* **12** 24503–9

[49] Xu Y, Liu W, Huang Y, Jin C, Zhou B, Sun J and Yang J 2021 Recent advances in flexible organic synaptic transistors *Adv. Electron. Mater.* **7** 2100336

[50] Sulzbach M C, Estandía S, Gàzquez J, Sánchez F, Fina I and Fontcuberta J 2020 Blocking of conducting channels widens window for ferroelectric resistive switching in interface-engineered $Hf_{0.5}$ $Zr_{0.5}$ $O_2$ tunnel devices *Adv. Funct. Mater.* **30** 2002638

[51] Zhang G, Ma C, Wu X, Zhang X, Gao C, Chen H and Guo T 2022 Transparent organic nonvolatile memory and volatile synaptic transistors based on floating gate structure *IEEE Electron Device Lett.* **43** 733–6

[52] Seo D G *et al* 2019 Versatile neuromorphic electronics by modulating synaptic decay of single organic synaptic transistor: from artificial neural networks to neuro-prosthetics *Nano Energy* **65** 104035

[53] G-T G, Lee Y, Seo D-G, Pei M, Lee W, Yang H and Lee T-W 2020 Achieving microstructure-controlled synaptic plasticity and long-term retention in ion-gel-gated organic synaptic transistors *Adv. Intell. Syst.* **2** 2000012

[54] Kim N *et al* 2023 Molecular tailoring to achieve long-term plasticity in organic synaptic transistors for neuromorphic computing *Adv. Intell. Syst.* **5** 2300016

[55] Izhikevich E M 2003 Simple model of spiking neurons *IEEE Trans. Neural Netw.* **14** 1569–72

[56] Otto J F, Yang Y, Frankel W N, White H S and Wilcox K S 2006 A spontaneous mutation involving Kcnq2 (Kv7.2) reduces M-current density and spike frequency adaptation in mouse CA1 neurons *J. Neurosci.* **26** 2053–9

[57] Ungless M A, Gasull X and Walters E T 2002 Long-term alteration of S-type potassium current and passive membrane properties in aplysia sensory neurons following axotomy *J. Neurophysiol.* **87** 2408–20

[58] Zhu Y *et al* 2022 Side-chain engineering of polystyrene dielectrics toward high-performance photon memories and artificial synapses *Chem. Mater.* **34** 6505–17

[59] Bronstein H, Nielsen C B, Schroeder B C and McCulloch I 2020 The role of chemical design in the performance of organic semiconductors *Nat. Rev. Chem.* **4** 66–77

[60] Spiess H W 2020 Improving organisation of discotics: annealing, shape, side groups, chirality *Liq. Cryst.* **47** 1880–5

[61] Zhao Y *et al* 2022 Side chain engineering enhances the high-temperature resilience and ambient stability of organic synaptic transistors for neuromorphic applications *Nano Energy* **104** 107985

[62] Gu J D, Ford T E and Mitchell R 1996 Susceptibility of electronic insulating polyimides to microbial degradation *J. Appl. Polym. Sci.* **62** 1029–34

[63] Sirringhaus H 2009 Reliability of organic field-effect transistors *Adv. Mater.* **21** 3859–73

[64] Li D, Borkent E J, Nortrup R, Moon H, Katz H and Bao Z 2005 Humidity effect on electrical performance of organic thin-film transistors *Appl. Phys. Lett.* **86** 042105

[65] Park Y D, Lim J A, Lee H S and Cho K 2007 Interface engineering in organic transistors *Epilepsy Behav.* **10** 84–8

[66] Ji D, Li L, Fuchs H and Hu W 2021 Engineering the interfacial materials of organic field-effect transistors for efficient charge transport *Acc. Mater. Res.* **2** 159–69

[67] Pei M *et al* 2020 Semiconductor/dielectric interface in organic field-effect transistors: charge transport, interfacial effects, and perspectives with 2D molecular crystals *Adv. Phys.* X **5** 1710252

[68] Jung U, Kim M, Jang J, Bae J, Kang I M and Lee S 2023 Formation of cluster-structured metallic filaments in organic memristors for wearable neuromorphic systems with bio-mimetic synaptic weight distributions *Adv. Sci.* **11** 2307494

[69] Wang H, Yang M, Tong Y, Zhao X, Tang Q and Liu Y 2019 Manipulating the hysteresis via dielectric in organic field-effect transistors toward synaptic applications *Org. Electron.* **73** 159–65

[70] Wu X, Chu Y, Liu R, Katz H E and Huang J 2017 Pursuing polymer dielectric interfacial effect in organic transistors for photosensing performance optimization *Adv. Sci.* **4** 1700442

[71] Shi J, Kang S, Feng J, Fan J, Xue S, Cai G and Zhao J S 2023 Evaluating charge-type of polyelectrolyte as dielectric layer in memristor and synapse emulation *Nanoscale Horiz.* **8** 509–15

[72] Lee S H, Park H L, Kim M H, Kim M H, Park B G and Lee S D 2020 Realization of biomimetic synaptic functions in a one-cell organic resistive switching device using the diffusive parameter of conductive filaments *ACS Appl. Mater. Interfaces* **12** 51719–28

[73] Yu Y *et al* 2019 Small-molecule-based organic field-effect transistor for nonvolatile memory and artificial synapse *Adv. Funct. Mater.* **29** 1904602

[74] Dong L, Chiu Y-C, Chueh C-C, Yu A-D and Chen W-C 2014 Semi-conjugated acceptor-based polyimides as electrets for nonvolatile transistor memory devices *Polym. Chem.* **5** 6834–46

[75] Jung M-H, Song K H, Ko K C, Lee J Y and Lee H 2010 Nonvolatile memory organic field effect transistor induced by the steric hindrance effects of organic molecules *J. Mater. Chem.* **20** 8016

[76] Zhang L, Wu T, Guo Y, Zhao Y, Sun X, Wen Y, Yu G and Liu Y 2013 Large-area, flexible imaging arrays constructed by light-charge organic memories *Sci. Rep.* **3** 1080

[77] Wang L, Zheng C, Fu J, Hua J, Chen J, Gao J, Ling H, Xie L and Huang W 2022 Influence of molecular weight of polymer electret on the synaptic organic field-effect transistor performance *Adv. Electron. Mater.* **8** 2200155

[78] Park H L, Kim M H, Kim H and Lee S H 2021 Self-selective organic memristor by engineered conductive nanofilament diffusion for realization of practical neuromorphic system *Adv. Electron. Mater.* **7** 2001219

[79] Verploegen E, Mondal R, Bettinger C J, Sok S, Toney M F and Bao Z 2010 Effects of thermal annealing upon the morphology of polymer-fullerene blends *Adv. Funct. Mater.* **20** 3519–29

[80] Du B, Yi J, Yan H and Wang T 2021 Temperature induced aggregation of organic semiconductors *Chem. Eur. J.* **27** 2908–19

[81] Yao Z F, Wang Z Y, Wu H T, Lu Y, Li Q Y, Zou L, Wang J Y and Pei J 2020 Ordered solid-state microstructures of conjugated polymers arising from solution-state aggregation *Angew. Chem., Int. Ed.* **59** 17467–71

[82] Kim S, Heo K, Lee S, Seo S, Kim H, Cho J, Lee H, Lee K B and Park J H 2021 Ferroelectric polymer-based artificial synapse for neuromorphic computing *Nanoscale Horiz.* **6** 139–47

[83] Yang Q, Huang J, Chen Q, Chen C, Chen H and Guo T 2022 Synaptic transistor with tunable synaptic behavior based on a thermo-denatured polar polymer material *J. Mater. Chem.* C **10** 5534–41

[84] Han H, Xu Z, Guo K, Ni Y, Ma M, Yu H, Wei H, Gong J, Zhang S and Xu W 2020 Tunable synaptic plasticity in crystallized conjugated polymer nanowire artificial synapses *Adv. Intell. Syst.* **2** 1900176

[85] Ke Y, Yu R, Lan S, He L, Yan Y, Yang H, Shan L, Chen H and Guo T 2021 Polymer bulk-heterojunction synaptic field-effect transistors with tunable decay constant *J. Mater. Chem.* C **9** 4854–61

[86] Park H L, Kim M H, Kim M H and Lee S H 2020 Reliable organic memristors for neuromorphic computing by predefining a localized ion-migration path in crosslinkable polymer *Nanoscale* **12** 22502–10

[87] Ding G, Zhao J, Zhou K, Zheng Q, Han S-T, Peng X and Zhou Y 2023 Porous crystalline materials for memories and neuromorphic computing systems *Chem. Soc. Rev.* **52** 7071–136

[88] Jeon Y J, An H, Kim Y, Jeon Y P and Kim T W 2021 Highly reliable memristive devices with synaptic behavior via facilitating ion transport of the zeolitic imidazolate framework-8 embedded into a polyvinylpyrrolidone polymer matrix *Appl. Surf. Sci.* **567** 150748

[89] Song Z, Tong Y, Zhao X, Ren H, Tang Q and Liu Y 2019 A flexible conformable artificial organ-damage memory system towards hazardous gas leakage based on a single organic transistor *Mater. Horiz.* **6** 717–26

[90] Broccard F D, Joshi S, Wang J and Cauwenberghs G 2017 Neuromorphic neural interfaces: from neurophysiological inspiration to biohybrid coupling with nervous systems *J. Neural Eng.* **14** 041002

[91] Lee H-S, J-S R, Ko G-M and Park H-L 2023 Flexible and stretchable synaptic devices for wearable neuromorphic electronics *Flex. Print. Electron.* **8** 043001

[92] de Moraes Porto I C C 2012 Polymer biocompatibility *Polymerization* (https://doi.org/10.5772/47786)

[93] Fahlman M, Fabiano S, Gueskine V, Simon D, Berggren M and Crispin X 2019 Interfaces in organic electronics *Nat. Rev. Mater.* **4** 627–50

[94] Riveiro A, Maçon A L B, Del Val J, Comesaña R and Pou J 2018 Laser surface texturing of polymers for biomedical applications *Front. Phys.* **6** 16

[95] Šafaříková E, Švihálková Šindlerová L, Stříteský S, Kubala L, Vala M, Weiter M and Víteček J 2018 Evaluation and improvement of organic semiconductors' biocompatibility towards fibroblasts and cardiomyocytes *Sens. Actuators* B **260** 418–25

[96] Yuk H, Lu B and Zhao X 2019 Hydrogel bioelectronics *Chem. Soc. Rev.* **48** 1642–67

[97] Kim Y *et al* 2018 A bioinspired flexible organic artificial afferent nerve *Science* **360** 998–1003
[98] Ren Y, Yang J, Zhou L, Mao J, Zhang S, Zhou Y and Han S 2018 Gate-tunable synaptic plasticity through controlled polarity of charge trapping in fullerene composites *Adv. Funct. Mater.* **28** 1805599
[99] Aimi J, Lo C, Wu H, Huang C, Nakanishi T, Takeuchi M and Chen W 2016 Phthalocyanine-cored star-shaped polystyrene for nano floating gate in nonvolatile organic transistor memory device *Adv. Electron. Mater.* **2** 1500300
[100] Chang H-C, Lee W-Y, Tai Y, Wu K-W and Chen W-C 2012 Improving the characteristics of an organic nano floating gate memory by a self-assembled monolayer *Nanoscale* **4** 6629
[101] Fu Y, Kong L, Chen Y, Wang J, Qian C, Yuan Y, Sun J, Gao Y and Wan Q 2018 Flexible neuromorphic architectures based on self-supported multiterminal organic transistors *ACS Appl. Mater. Interfaces* **10** 26443–50
[102] Wu C, Kim T W, Choi H Y, Strukov D B and Yang J J 2017 Flexible three-dimensional artificial synapse networks with correlated learning and trainable memory capability *Nat. Commun.* **8** 752